NDT&E International 71 (2015) 1–7

Contents lists available at ScienceDirect

NDT&E International

journal homepage: www.elsevier.com/locate/ndteint

In-situ monitoring of fatigue crack growth using high frequency guided waves

B. Masserey [a], P. Fromme [b,*]

[a] Department of Mechanical Engineering, University of Applied Sciences, Fribourg, Switzerland
[b] Department of Mechanical Engineering, University College London, London WC1E 7JE, UK

ARTICLE INFO

Article history:
Received 27 October 2014
Received in revised form
13 December 2014
Accepted 19 December 2014
Available online 29 December 2014

Keywords:
Fatigue crack
Monitoring
High frequency guided ultrasonic waves
P/E measurement
Lamb wave modes

ABSTRACT

The development of fatigue cracks at fastener holes represents a common maintenance problem for aircraft. High frequency guided ultrasonic waves allow for the monitoring of critical areas without direct access to the defect location. During cyclic loading of tensile, aluminum specimens fatigue crack growth at the side of a fastener hole was monitored. The changes in the energy ratio of the baseline subtracted reflected guided wave signal due to the fatigue damage were monitored from a stand-off distance using standard ultrasonic pulse–echo measurement equipment. Good sensitivity for the detection and monitoring of fatigue crack growth was found.

1. Introduction

The development of fatigue cracks at fastener holes in aluminum components is a common maintenance problem for the aircraft industry [1]. Especially the development of widespread fatigue damage due to stress concentration and cyclic loading conditions constitutes a safety-critical problem for ageing aircraft [2]. Different nondestructive testing (NDT) methods have been developed for the early detection of fatigue cracks [3]. Some of them require direct access to the inside of the fastener hole [3], complicating the possible integration into a structural health monitoring (SHM) system. Ultrasonic bulk wave measurements have a proven track record and sensitivity for the detection and sizing of cracks [4]. The real time, in-situ monitoring of fatigue cracks at fastener holes using an angle beam through transmission technique has been demonstrated [5]. However, bulk wave ultrasonic testing necessitates local access to the damaged area of the inspected structure.

Guided ultrasonic waves have been proposed for the integration into SHM systems, as with appropriate mode selection they offer the required area coverage [6]. Most work has focused on the selective excitation of one of the fundamental modes (A_0 and S_0 Lamb wave modes) below the cut-off frequencies of the higher wave modes [7], as this allows simpler signal interpretation and typically lower attenuation for realistic aircraft structures [8]. The scattering of guided waves at a hole with and without a fatigue crack has been investigated [9]. Guided waves have been successfully employed to detect and monitor fatigue crack growth in metallic structures [10], and this has been extended for the monitoring of a series of through holes with multiple crack initiation sites [1]. However, low frequency guided waves have a wavelength significantly larger than in bulk wave ultrasonic testing, ultimately limiting the sensitivity for the detection of small defects [11]. The shorter wavelengths of surface acoustic waves propagating along a structure have been employed for enhanced fatigue crack monitoring sensitivity [12].

High frequency guided ultrasonic waves offer an interesting compromise between the proven defect detection sensitivity of bulk ultrasonic waves and achievable propagation range. Different modes and frequency-thickness operating ranges have been investigated for defect detection over medium long distances, e.g., for corrosion detection in aircraft panels [13] and defects in plate structures [14]. With the appropriate choice of wave mode excitation good detection sensitivity for small surface defects and the potential to differentiate the damaged plate side have been demonstrated [15]. Previous work has found good sensitivity for the early detection and monitoring of fatigue crack growth during cyclic loading using noncontact laser measurements close to the damage location [16]. The two fundamental Lamb wave modes were excited selectively at a frequency-thickness product of 6.75 MHz mm, significantly above the cut-off frequencies of the higher Lamb wave modes [17]. The scattering of this type of high frequency guided waves from fatigue cracks at a

* Corresponding author. Tel.: +44 207 679 3944.
E-mail address: p.fromme@ucl.ac.uk (P. Fromme).

http://dx.doi.org/10.1016/j.ndteint.2014.12.007
0963-8695/

fastener hole had been previously measured and compared to numerical predictions in order to understand and quantify the potential detection sensitivity [18].

This contribution extends this work to the experimental in-situ monitoring of fatigue crack growth in tensile, aluminum specimens from a stand-off distance from the fastener hole without direct, local access to the damage. The high frequency guided waves were excited using a standard angle beam transducer and monitored using standard ultrasonic pulse–echo equipment. The fatigue crack growth was measured optically during cyclic loading and the changes in the reflected high frequency guided ultrasonic wave pulse were quantified. Calculating the energy ratio of the time-gated and baseline subtracted guided wave reflected pulse–echo (P/E) signal, good sensitivity of the measured changes with crack size were confirmed.

2. High frequency guided ultrasonic wave propagation

High frequency guided waves represent a compromise between achievable propagation distance along plate structures and sensitivity for the detection of small defects due to their relative short wavelength [14]. For this investigation the fundamental anti-symmetric (A_0) and symmetric (S_0) Lamb modes at a frequency-thickness region of about 6.75 MHz mm were excited in a plate (center frequency of 2.25 MHz for a 3 mm thick structure). These modes are easily generated and received with sufficient selectivity above the cut-off frequencies of the higher Lamb wave modes using standard angle beam transducers [17]. In this frequency region the wavelength equals approximately half of the plate thickness and the A_0 and S_0 modes have modeshapes with stress and displacement fields similar to a Rayleigh wave on each plate surface. However, for excitation on the upper surface there is small residual amplitude at the lower boundary, causing a coupling between the two surfaces. This gives rise to an energy transfer from one side of the plate to the other and then back over a distance called the beatlength [19]. The beatlength L can be calculated as

$$L = \frac{2\pi}{k_{A_0} - k_{S_0}}, \tag{1}$$

where k_{A_0} and k_{S_0} are the wave numbers of the fundamental anti-symmetric and symmetric Lamb modes. The beatlength depends on the difference between the wave numbers k_{A_0} and k_{S_0} in the denominator term. With increasing frequency the difference between wave numbers decreases and thus the beatlength increases. For a frequency of 2.25 MHz mm the difference in wave number (and thus phase velocity) between the fundamental anti-symmetric and symmetric Lamb modes is about 0.5%, resulting in a beatlength $L=250$ mm for a 3 mm thick aluminum plate. The associated beating phenomenon can be used for the detection of small cracks on both plate sides with single-sided access or, selecting appropriate excitation frequency and position, for the inspection of structures where access is restricted by regularly spaced features such as stiffeners or stringers [17].

Fig. 1 shows the group velocity dispersion diagram for the used 3 mm thick aluminum plate specimens. The group velocities of the fundamental Lamb wave modes (A_0 and S_0) are shown as solid lines. These have been widely employed for SHM applications in large structures at low frequencies [6]. In the frequency range of interest around 2.25 MHz the fundamental modes are rather non-dispersive and the velocities start to converge towards the Rayleigh wave velocity (2918 m/s). The group velocity of the A_0 mode for 2.25 MHz at 2948 m/s is slightly higher than the group velocity of the S_0 mode at 2879 m/s, resulting in a relative difference of the expected arrival times of about 2.5%.

3. Experiments

Five tensile specimens with length 600 mm, width 70 mm, and thickness 3 mm (Fig. 2), made of aluminum alloy 2014 T6, were used for the fatigue testing. A 1/4 in. diameter hole ($r=3.17$ mm) was drilled on the center line at 200 mm from the specimen end (Fig. 2). The specimens were subjected to cyclic tensile loading in a servo-hydraulic testing machine (Fig. 3(a)) with the axis of loading along the specimen length. A maximum load of 26 kN with stress ratio $R=0.1$ and a cycling frequency of 10 Hz were selected. The maximum stress in the vicinity of the hole (stress concentration factor $K_t=2.75$) was significantly above the fatigue strength of the aluminum alloy, but just below the yield limit in order to avoid plastic deformation. A small triangular starter notch, approximately 0.2 mm long, was made on one side of the specimen at the hole boundary (perpendicular to the loading axis) in order to prescribe the crack initiation location. During fatigue testing the crack grew quarter-elliptically from the starter notch position to a length and depth of about 3 mm. At that depth, corresponding to the specimen thickness, the crack quickly developed into a through-thickness crack.

The cyclic loading was paused every 1000 cycles and the specimen held under the maximum tensile load to avoid crack closure. The crack size was measured optically on the front surface (crack

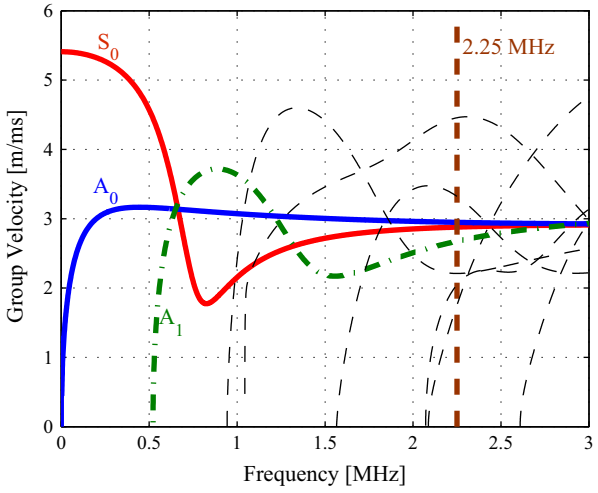

Fig. 1. Group velocity dispersion diagram for 3 mm thick aluminum plate (Al 2014 T6); fundamental modes (A_0 and S_0): solid lines; A_1 mode: dash-dotted line; higher order modes: dashed lines; center frequency 2.25 MHz marked.

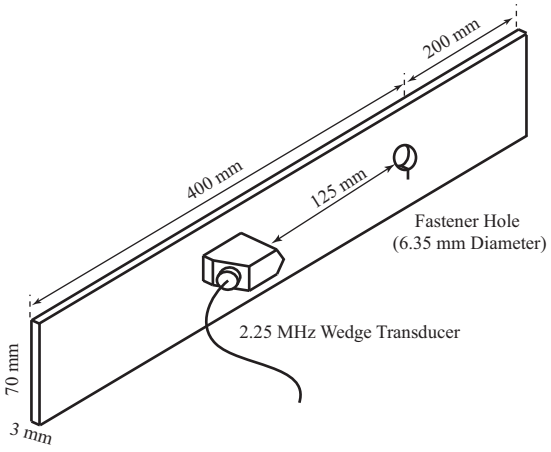

Fig. 2. Schematic of tensile specimen (Al 2014 T6, 600 mm × 70 mm × 3 mm) with fastener hole (1/4 in./6.35 mm diameter) and location of 2.25 MHz wedge transducer.

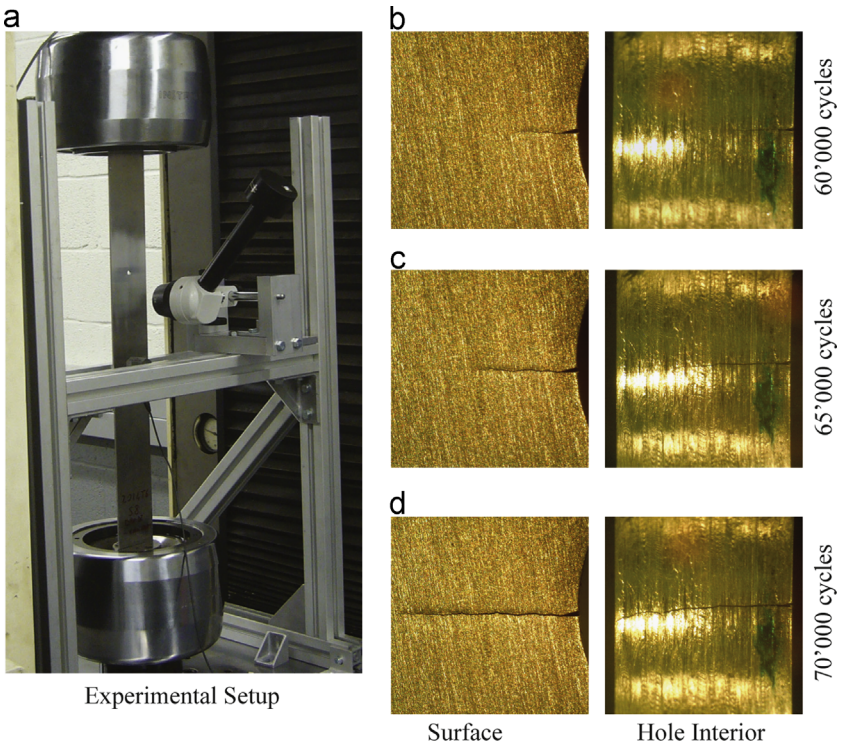

Fig. 3. (a) Photo of tensile specimen in hydraulic testing machine with microscope and transducer; photos of crack on specimen surface (left) and through hole interior (right): (b) 60,000 cycles, crack length 1.06 mm, crack depth 1.06 mm; (c) 65,000 cycles, crack length 1.81 mm, crack depth 2.01 mm; (d) 70,000 cycles, crack length 3.13 mm, through thickness.

length) and through the hole thickness (crack depth) by means of an optical microscope and a mirror inserted into the fastener hole. Once the fatigue crack had grown through the thickness, the length on the front and back surface of the specimen were measured and averaged to calculate the crack area (Fig. 4(b)). Crack initiation varied between the five specimens, but due to the identical loading conditions the fatigue crack growth was repeatable [16]. Typical pictures of the crack growth for one specimen are shown in Fig. 3(b)–(d). Fig. 3 (b) shows the small quarter-elliptical crack at 60,000 cycles with a length and depth of approximately 1 mm, corresponding to a crack area of 0.88 mm^2. For 65,000 cycles the quarter-elliptical crack had grown to a depth of about 2 mm with a corresponding area of 2.86 mm^2 (Fig. 3(c)). The through thickness crack can be seen in Fig. 3(d) at 70,000 cycles with a length on the front surface of 3.13 mm. The corresponding crack growth data as a function of the number of cycles is shown in Fig. 4. The crack was first observed optically at 52,000 cycles and had grown through the thickness at 68,000 cycles (Fig. 4(a)). The experimentally observed fatigue crack growth showed good agreement for crack depth and length with predictions of an analytical model based on Forman crack propagation law [16].

Standard ultrasonic pulse–echo (P/E) measurements were conducted from a stand-off distance to monitor the high frequency guided wave pulse reflected at the fastener hole and at the fatigue crack. Measurements were taken every 1000 cycles while the cyclic loading was paused and the specimen held under maximum load to avoid crack closure during the ultrasonic measurements. Further measurements should investigate the relevance of the load (and the resulting crack opening) on the ultrasonic signals and thus detection sensitivity for fatigue cracks. The guided wave pulse was excited and measured using a standard 90° angle beam transducer and wedge (Panametrics A540S/ABWML-5T-90°) with a center frequency of 2.25 MHz (Rayleigh wavelength in aluminum at 2.25 MHz: $\lambda_R = 1.3$ mm). As the wedge angle is optimized for steel rather than aluminum and the working

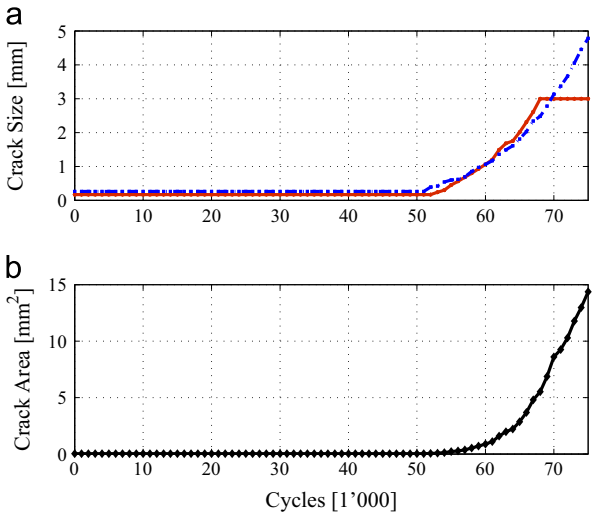

Fig. 4. Typically observed fatigue crack growth for same specimen as photos in Fig. 3; (a) optically measured crack length on specimen surface (dash-dotted) and crack depth in fastener hole interior (solid); (b) calculated crack area; shown against number of cycles.

frequency is significantly above the cut-off frequency of the higher Lamb wave modes (Fig. 1) it had been previously found that, besides the desired fundamental Lamb wave modes (A_0 and S_0), the first higher antisymmetric Lamb mode (A_1) was excited as well [15]. However, the amplitude of the A_1 mode was found to be only about 10% of the fundamental modes and due to the dispersion behavior (Fig. 1) the wave pulse spreads rapidly in time. In addition, as the group velocity of the A_1 mode is about 10% slower than for the A_0 mode it arrives significantly after the fundamental modes and can be time-gated out. The wedge was clamped to the tensile specimen (Fig. 3(a)) at a distance $d = 125$ mm from the hole center on the

specimen surface opposite to the surface where the starter notch was made (Fig. 2). The distance, corresponding to half a beatlength at center frequency ($L=250$ mm) [16], was selected in order to concentrate the energy next to the fastener hole on the specimen side containing the starter notch. The transducer was aligned along the specimen center line to maximize the reflection at the fastener hole and fatigue crack. The specimen width was sufficient so that the sides did not affect the wave propagation, but did not allow for the investigation of fatigue cracks at different angles around the fastener hole relative to the incident wave direction. If the transducer cannot be placed at an optimum location relative to the expected crack orientation (for the stress field) the influence on the detection sensitivity would have to be ascertained. Wave excitation and reception was performed using a standard ultrasonic pulser–receiver (Panametrics 5800) to allow for the P/E measurement using the inbuilt receiver circuitry. The excited wave pulse was found to be wideband up to approximately 3.5 MHz and the internal band-pass filter was set to 1–5 MHz around the transducer center frequency. The received signals were averaged (100 averages) and recorded using a digital storage oscilloscope (LeCroy 9304).

4. P/E measurement of fatigue crack growth

The time traces resulting from the pulse–echo measurement at a stand-off distance from the fastener hole for the same specimen as in Fig. 3 are shown in Fig. 5. The baseline signal in Fig. 5(b) shows the reflection at the undamaged fastener hole at the start of the cyclic loading. The zoom of the clear and strong reflected pulse is shown in Fig. 5(a). The waveform is characterized by a distinct dispersive behavior. The use of a wideband excitation leads to a partial separation in time of the A_0 and S_0 Lamb wave modes. The arrival time of the front of the reflected pulse at about 108 μs matches the addition of the predicted propagation time in the wedge with the longitudinal velocity in Perspex and in the specimen with the fastest group velocity for the low frequency part of the A_0 mode, propagating with a group velocity slightly higher than the Rayleigh wave velocity. The expected arrival time for the S_0 mode is about 2 μs later and no time separation of the pulses is visible in Fig. 5(a). The main pulse includes both interfering fundamental modes A_0 and S_0. The pulse at about 113 μs and the following pulses are mainly the low frequency part of the S_0 mode characterized by a group velocity smaller than the Rayleigh wave velocity. The arrival time of the A_1 mode would be about 9 μs later and as expected no significant pulse at 117 μs was detected. The time signal shows some amplitude variation between 107 and 120 μs, which was consistent between the baseline measurements for the different specimens. Small variations were observed for the initial measurements, possibly due to the settling of the clamped wedge relative to the specimen, and the first two recorded time traces at 0 and 1000 cycles were discarded. For each specimen, the signal averaged from the next 10 measurements (2000–11,000 cycles) was taken as the baseline signal. Some small changes in the arrival time of the pulses (up to about 10% of signal period) were observed before crack initiation, mostly correlated to longer stoppage of the experiments overnight. Therefore, an automatic correction to re-align the pulses was implemented in Matlab, using the cross-correlation of the initial reflection of the A_0 mode at the fastener hole from 107 to 110 μs. As the expected arrival time of the first reflection at the fatigue crack is about 2.5 μs later, it was assumed that this part of the pulse was not affected, which was confirmed from visual observation of the reflected pulses.

Fig. 5(c) shows the reflected time signal recorded for this specimen at 60,000 cycles, 8000 cycles after the fatigue crack was first visually observed. For a crack length and depth of about 1 mm a change in the pulse shape with an increase of reflected amplitude in the later part of the signal can be seen. This change in signal shape and amplitude increased with growing size of the quarter-elliptical crack, as shown for a crack depth of about 2 mm at 65,000 cycles in Fig. 5(e). Once the crack had grown through the specimen thickness a strong reflected pulse was seen as shown in Fig. 5(g). It should be noted that the observed changes in the reflected signal varied to some degree between the different specimens, especially for larger crack areas, e.g., not for all specimens such a large reflected amplitude as in Fig. 5(g) was seen. As the reflected signals consist of an overlap of wave pulses from different guided wave modes and reflections at the hole and at the fatigue crack, small changes in the location and shape of the fatigue crack can lead to relative phase shifts and thus constructive/destructive interferences of the different pulses. It was therefore decided to perform a baseline subtraction [18] of the reflected wave pulse relative to the baseline signal (averaged of 10 measurements). This allowed for the separation of the changes in the reflected field due to the crack from the direct reflection at the hole. The resulting signal is shown in Fig. 5(d) for the 1 mm long crack at 60,000 cycles. The time delay of about 2.5 μs relative to the baseline signal corresponds to the additional propagation distance to the fatigue crack location. With increasing crack size a significant increase in the signal difference can be seen in Fig. 5(f) for a 2 mm deep crack at 65,000 cycles and for a through thickness crack at 70,000 cycles in Fig. 5(h).

5. Energy evaluation of fatigue crack monitoring

The analysis of the measured P/E time traces has shown that the relevant parameter for detection sensitivity is the modification of the measured waveform due to the additional high frequency guided wave arising from the reflection at the crack, separated using a baseline subtraction. The time traces shown in Fig. 5(c)–(g) shows a change in the pulse shape with an increase of reflected amplitude in the later part of the signal. Potentially a fatigue crack could have been detected just from the change in the P/E time signal by itself. However, an energy ratio method similar to [16] was applied to allow a simple quantification of the relative change in the baseline subtracted signal and easier interpretation. This procedure was found to be more reliable than, for example, the maximum pulse amplitude, due to the interference of the different wave pulses. The energy parameter E_n at cycle n was defined as the addition of the energy parameter E_0 of the baseline measurement and the energy parameter E_n^* of the waveform at cycle n after baseline subtraction. This parameter was calculated within a windowed portion of the signal that extended from time $t_0=107$ μs to $t_1=120$ μs containing the complete reflected pulse as explained above. The energy ratio R was obtained by normalizing the energy parameter E_n with the baseline parameter E_0:

$$R=\frac{E_n}{E_0}=1+\frac{E_n^*}{E_0}, \tag{2}$$

with

$$E_0=\int_{t_0}^{t_1}(x_0(t))^2dt, E_n^*=\int_{t_0}^{t_1}(x_n^*(t))^2dt, \tag{3}$$

where t is time, $x_0(t)$ is the baseline signal and $x_n^*(t)$ is the waveform at cycle n after baseline subtraction.

Fig. 6(a) shows the calculated energy ratio for the 5 tensile specimens, with Fig. 6(b) giving a magnification of the same data for small crack sizes. The ultrasonic P/E measurement every 1000 cycles was evaluated as described above and the energy ratio was plotted against the optically measured crack area. The initial crack area corresponds to the length and depth of the starter notch, which varied slightly between specimens. Crack initiation was detected optically at crack lengths varying between 0.26 mm and 0.42 mm for the different tensile specimens. Before optical detection, the energy ratio was plotted as if occurring at the area of the starter notch and

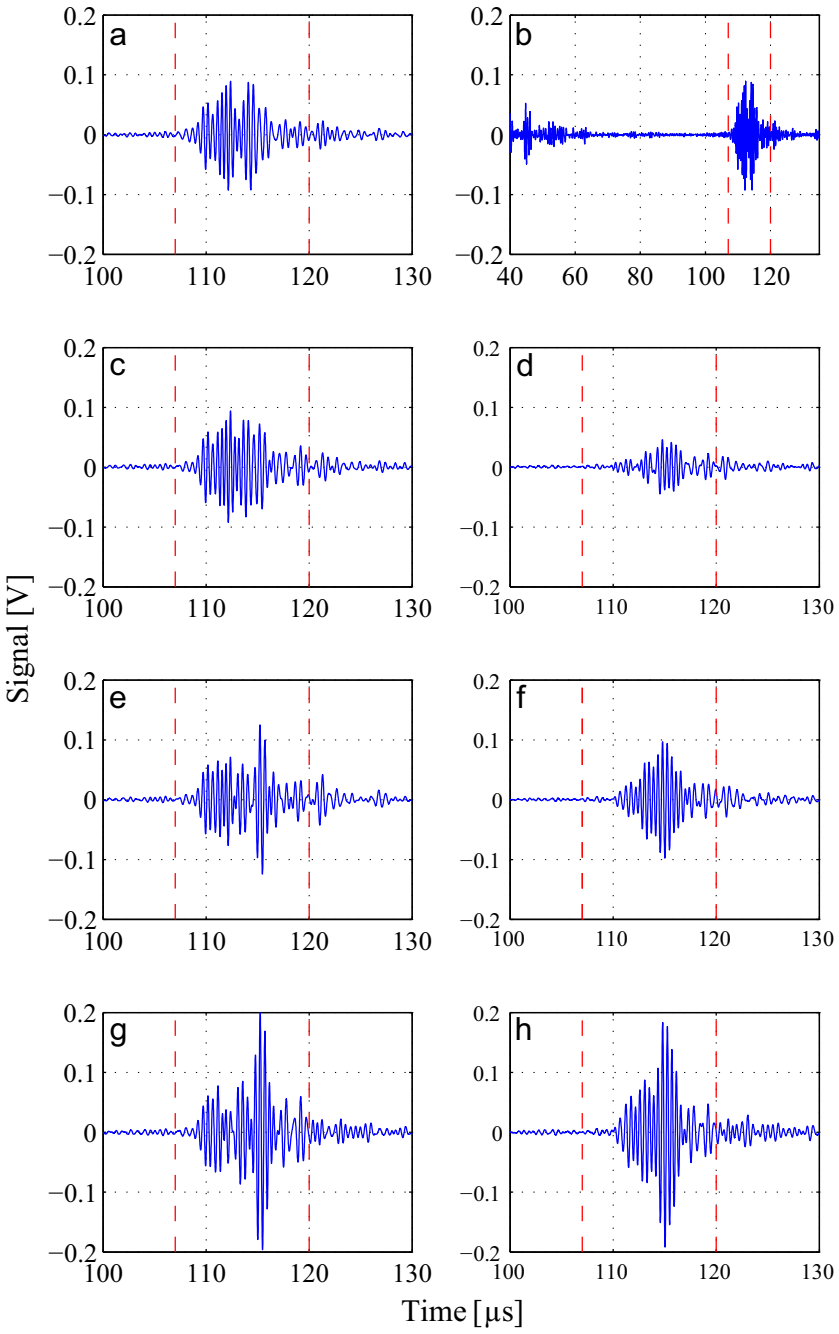

Fig. 5. Measured P/E time traces and baseline subtracted signal differences (time window 107–120 μs shown); (a) zoom of signal for 10,000 cycles, no crack (baseline); (b) signal for 10,000 cycles; (c) signal for 60,000 cycles, crack length 1.06 mm, crack depth 1.06 mm; (d) signal difference for 60,000 cycles; (e) signal for 65,000 cycles, crack length 1.81 mm, crack depth 2.01 mm; (f) signal difference for 65,000 cycles; (g) signal for 70,000 cycles, crack length 3.13 mm, through thickness; (h) signal difference for 70,000 cycles.

taken as the uncertainty in the measurements. The largest observed variation in the energy ratio before a fatigue crack was visually detected was 7.3% for one specimen (dash-dotted line), with smaller values from 1.8% to 6.5% for the other 4 specimens. The energy ratio increases with increasing crack area, but at slightly different rates for the five specimens. A conservative threshold of 15% increase in the energy ratio was set as twice the maximum variation of 7.3% (Fig. 6(b)). For all specimens an increase in energy ratio of more than 15% was observed for a crack area of 0.8 mm^2 or less. For individual specimens smaller cracks could potentially be detected, but it would not be possible to set specific threshold limits in advance. The crack detection threshold of 0.8 mm^2 corresponds approximately to a crack length and depth of 1 mm (approximately 75% of the Rayleigh wavelength in aluminum), similar to the crack at 60,000 cycles shown in Fig. 3(b).

The energy ratio continues to increase with growing crack area. For a crack area of up to 2 mm^2 reasonably similar behavior of the curves for the five different specimens can be observed in Fig. 6(a), even though some differences are evident in the magnification in Fig. 6(b). For small fatigue cracks this might in principle allow an approximate sizing of the crack area from the calculated energy ratio, but with rather large uncertainties. For larger fatigue cracks (>2 mm^2 in Fig. 6(a)) different rates for the correlation of the energy ratio to the crack can be observed. For 3 of the specimens the increase with crack area is larger than for the other 2 specimens, making crack sizing impossible. The increased energy ratios matched the observed changes in the time

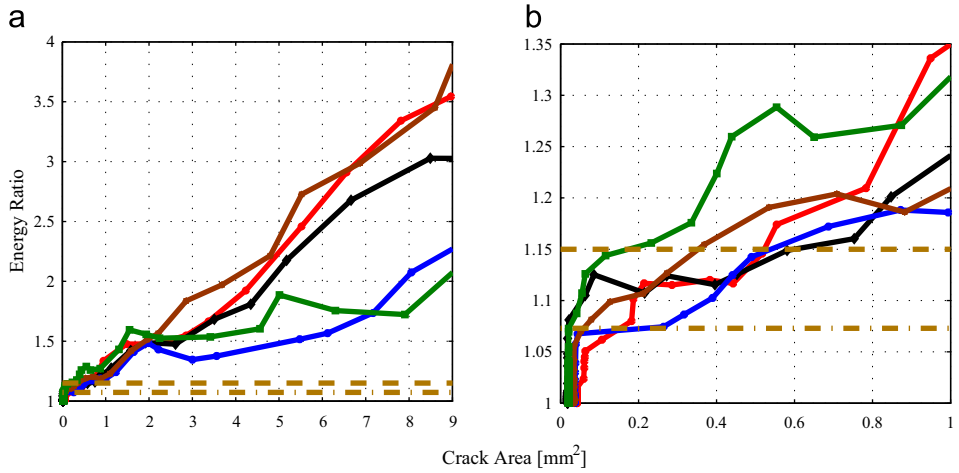

Fig. 6. (a) Energy ratio of reflected P/E signal for 5 tensile specimens against optically measured crack area (solid lines); time window 107–120 μs; (b) zoom for small crack area; 7.3% maximum variation before visual crack observation (dash-dotted); 15% threshold (dashed).

traces, e.g., significantly larger amplitude changes for some of the specimens compared to the others. No apparent reason for this was observed during the fatigue testing and during the evaluation procedure, but the variation between the curves for large fatigue cracks can possibly be associated to small differences in crack location and shape between the measurements. This modifies the interferences between the A_0 and S_0 modes reflected at the crack and fastener hole and affects the P/E measurement. The selection of the energy ratio as the detection parameter allows a simple quantification of the fatigue crack influence on the reflected signal and thus comparison between specimens and setting of a conservative threshold for which small fatigue cracks can be detected from a stand-off distance.

6. Conclusions

The detection and monitoring of fatigue crack growth at fastener holes in aircraft structures presents a significant maintenance problem, where cracks need to be detected before they have reached a safety critical size. Due to their relative short wavelength, high frequency guided waves represent a compromise between achievable propagation distance along thin aerospace structures and sensitivity for the detection of small defects. For the integration into SHM systems the sensitivity and reliability of defect detection needs to be ascertained. Previous contributions have demonstrated the effect of a fatigue crack on the scattered wave field and the good sensitivity for the early detection and monitoring of fatigue crack growth employing noncontact measurements using a laser interferometer close to the fastener hole and fatigue crack location. This investigation demonstrated the potential for practical measurements by means of standard ultrasonic pulse–echo equipment at a stand-off distance from the fastener hole without direct access to the damage location. Employing a standard ultrasonic wedge transducer clamped at a stand-off distance from the damage location, the combined reflection at the fastener hole and fatigue crack was measured. The P/E signal contains the superposition of the fundamental high frequency guided wave modes (A_0 and S_0 Lamb modes), which overlap in time. The calculation of the energy ratio of the baseline subtracted and time gated signals was employed to quantify the observed changes with fatigue crack growth. Using a conservative limit of twice the maximum observed variation in the energy for any of the five tested specimens, fatigue cracks with an area of less than 0.8 mm^2, corresponding approximately to a crack length and depth of 1 mm, could be reliably detected. Due to the varying interference between the different reflected guided wave pulses the change in the time signals and thus rate of increase in the energy ratio with increasing crack size varied, especially for larger fatigue cracks. This makes a direct correlation of the energy ratio to the crack size difficult. Further studies should be performed to investigate this further, as well as to understand the influence of load and temperature on the observed signal changes and the applicability of the methodology for complex, multi-layered aircraft structures.

Acknowledgements

This work was partially supported by the UK Engineering and Physical Sciences Research Council (EPSRC) (grant number EP/D065011/1).

References

[1] Cho H, Lissenden CJ. Structural health monitoring of fatigue crack growth in plate structures with ultrasonic guided waves. Struct Health Monit 2012;11:393–404.
[2] Pitt S, Jones R. Multiple-site and widespread fatigue damage in aging aircraft. Eng Fail Anal 1997;4:237–57.
[3] Papazian JM, Nardiello J, Silberstein RP, Welsh G, Grundy D, Craven C, et al. Sensors for monitoring early stage fatigue cracking. Int J Fatigue 2007;29:1668–80.
[4] Cobb AC, Michaels JE, Michaels TE. An automated time–frequency approach for ultrasonic monitoring of fastener hole cracks. NDT E Int 2007;40:525–36.
[5] Michaels JE, Michaels TE, Mi B. An ultrasonic angle beam method for in situ sizing of fastener hole cracks. J Nondestr Eval 2006;25:3–16.
[6] Wilcox PD, Lowe MJS, Cawley P. Mode and transducer selection for long range Lamb wave inspection. J Intell Mater Syst Struct 2001;12:553–65.
[7] Fromme P, Wilcox PD, Lowe MJS, Cawley P. On the development and testing of a guided ultrasonic wave array for structural integrity monitoring. IEEE Trans Ultrason Ferroelectr Freq Control 2006;53:777–85.
[8] Dalton RP, Cawley P, Lowe MJS. The potential of guided waves for monitoring large areas of metallic aircraft fuselage structures. J Nondestr Eval 2001;20:29–46.
[9] Fromme P, Sayir MB. Detection of cracks at rivet holes using guided waves. Ultrasonics 2002;40:199–203.
[10] Leong WH, Staszewski WJ, Lee BC, Scarpa F. Structural health monitoring using scanning laser vibrometry: III. Lamb waves for fatigue crack detection. Smart Mater Struct 2005;14:1387–95.
[11] Alleyne DN, Cawley P. The interaction of Lamb waves with defects. IEEE Trans Ultrason Ferroelectr Freq Control 1992;39:381–97.
[12] Connolly GD, Rokhlin SI. Enhancement of fatigue crack monitoring by surface acoustic wave reflection and modulation in a space-cycle-load domain: an imaging approach. Struct Health Monit 2012;11:187–96.
[13] Terrien N, Osmont D, Royer D, Lepoutre F, Déom A. A combined finite element and modal decomposition method to study the interaction of Lamb modes with micro-defects. Ultrasonics 2007;46:47–78.
[14] Greve DW, Zheng P, Oppenheim IJ. The transition from Lamb waves to longitudinal waves in plates. Smart Mater Struct 2008;17:035029.
[15] Masserey B, Fromme P. On the reflection of coupled Rayleigh-like waves at surface defects in plates. J Acoust Soc Am 2008;123:88–98.

[16] Masserey B, Fromme P. Fatigue crack growth monitoring using high frequency guided waves. Struct Health Monit 2013;12:484–93.
[17] Masserey B, Fromme P. Surface defect detection in stiffened plate structures using Rayleigh-like waves. NDT E Int 2009;42:564–72.
[18] Masserey B, Fromme P. In-situ monitoring of fatigue crack growth at fastener holes using Rayleigh-like waves. In: Thompson DO, Chimenti DE, editors. Rev. of Prog. in QNDE 27B, AIP conference proceedings 975. New York; 2008. p. 1484–91.
[19] Ti BW, O'Brien WD, Harris JG. Measurements of coupled Rayleigh wave propagation in an elastic plate. J Acoust Soc Am 1997;102:1528–31.